Electronic Supplementary Material (ESI) for Journal of Materials Chemistry A.
This journal is © The Royal Society of Chemistry 2014

Supporting Information (S.I.).

Innovative high performing metal organic framework (MOF)-laden nanocomposite polymer electrolytes for all solid state lithium batteries

Claudio Gerbaldi[1,*], Jijeesh R. Nair[1,*], M. Anbu Kulandainathan[2], R. Senthil Kumar[2], Chiara Ferrara[3], Piercarlo Mustarelli[3] and Arul Manuel Stephan[2,*]

1) GAME Lab, Department of Applied Science and Technology – DISAT, Institute of Chemistry, Politecnico di Torino, C.so Duca degli Abruzzi 24, 10129 Torino, Italy.

2) Central Electrochemical Research Institute (CSIR-CECRI), Karaikudi 630 006, India.

3) Department of Chemistry, Section of Physical Chemistry, University of Pavia, and INSTM, Via Taramelli 16, Pavia, Italy

[*] Corresponding authors: Claudio Gerbaldi (claudio.gerbaldi@polito.it; PHONE: +39 011 090 4643; FAX: +39 011 090 4699; contact details: affiliation 1) and Arul Manuel Stephan (amstephan@cecri.res.in or arulmanuel@gmail.com; PHONE: +91 4565 241426; FAX: +91 4565 227779; contact details: affiliation 2).

Preparation of Al-BTC MOF

Al-plates with 99.9% purity (John Mathew, India) were used as the electrode materials. Benzene tricarboxylic acid (BTC Acros organics, India), supporting electrolytes like TBATFB - Tetrabutylammonium tetrafluoroborate, TEATFB - Tetraethylammonium tetrafluoroborate, TBAPC - Tetrabutylammonium perchlorate (Acros organics, India, analytical grade) and methanol (Sisco Research Laboratories, HPLC grade) were used as received for the synthesis of MOFs.

Two aluminium electrodes having similar area (10.5 cm^2) were used as the anode and the cathode for the synthesis of aluminium(III)-1,3,5,-benzenetricarboxylate (shortly, Al-BTC). Both the organic linker (0.1 M BTC) and the supporting electrolyte were dissolved in 50 ml methanol solution in the electrolysis cell and stirred for 15 min for complete dispersion. After proper optimisation of the reaction conditions (given in Table S1 & Fig. S1), electrolysis was carried out in an electrochemical cell under constant voltage for more than 2.5 h to complete the reaction (for the courtesy of the reader, it is schematically shown in Scheme S.1).

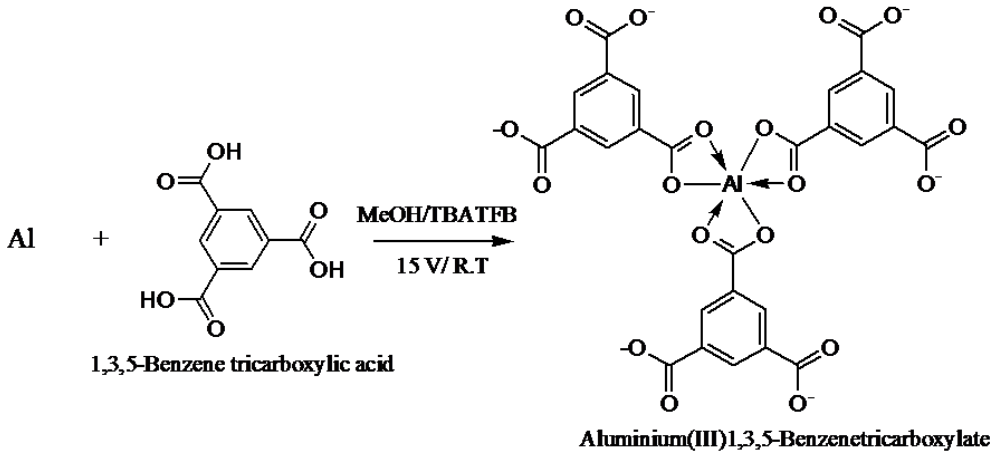

Scheme S.1. Reaction scheme for Al-BTC synthesis from Al and 1,3,5-benzene tricarboxylic acid.

Finally, the colourless precipitate of Al-BTC was collected from the electrolysis cell and allowed to dry in a hot air oven at 120 °C for 12 h and activated at 200 °C for 2 h. The obtained yield of the product corresponding to the amount of weight loss in the aluminium anode was 93.4 %.

Table S.1. Experimental parameters for the optimisation of the reaction conditions.

No.	Supporting Electrolyte (S.E.)	S.E. concentration (M)	BTC concentration (M)	Applied Cell Potential (V)	Yield (g)
1	TBATFB	0.1	0.1	15	0.57
2	TEATFB	0.1	0.1	15	No reaction
3	TBAPC	0.1	0.1	15	3.36
Effect of Supporting Electrolyte concentration					
4	TBAPC	0.02	0.1	15	0.32
5	TBAPC	0.04	0.1	15	0.75
6	TBAPC	0.05	0.1	15	2.78
7	TBAPC	0.2	0.1	15	1.93
Effect of BTC Concentration					
8	TBAPC	0.1	0.05	15	1.52
9	TBAPC	0.1	0.15	15	3.19
Effect of Applied Cell Potential					
10	TBAPC	0.1	0.1	5	0.56
11	TBAPC	0.1	0.1	10	1.67
12	TBAPC	0.1	0.1	12.5	1.92
13	TBAPC	0.1	0.1	17.5	1.95

where TBAPC - Tetrabutylammonium tetrafluoroborate, TEATFB - Tetraethylammonium tetrafluoroborate, TBAPC – Tetrabutylammonium perchlorate.

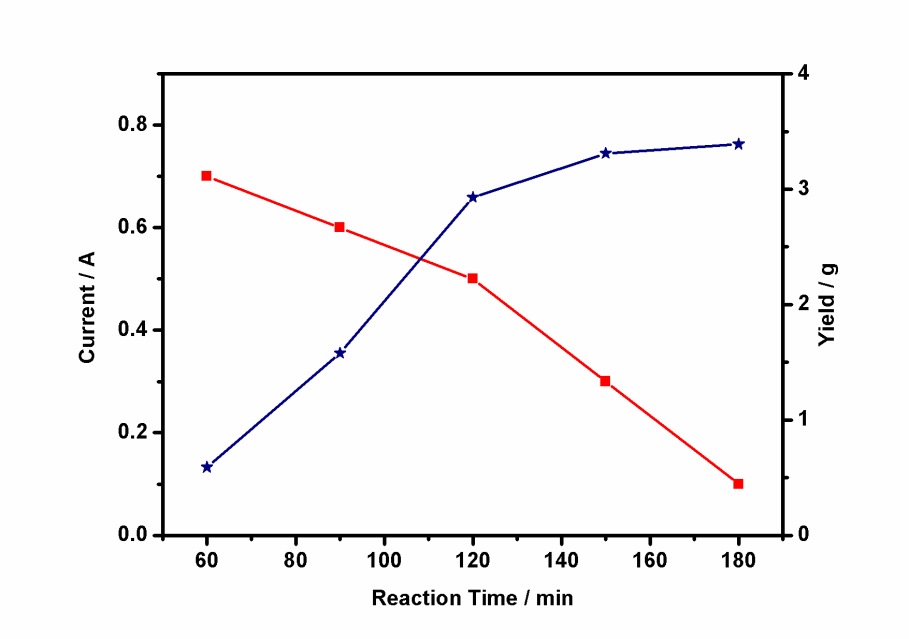

Figure S.1. The plots corresponding to the reaction time *vs.* yield and reaction time *vs.* current.

Final optimized conditions: 0.1M BTC / 0.1M TBAPC / 15 V / reaction time 150 min.

Characterisation techniques

Powder X-ray diffraction (XRD) analysis was performed on a Panalytical PW1140–PW3020 with Cu Kα X-ray radiation source (λ ≈ 1.54 Å). Morphological characterization of both the Al-BTC MOF products and the nanocomposite polymer electrolyte membranes was performed by a high resolution Field Emission Scanning Electron Microscope (FESEM, ZEISS MERLIN 4248) equipped with an OXFORD Energy Dispersive Spectroscopy Systems (EDS/EDX, having a X-ACT detector with a resolution of 130 eV at 5.9 KeV) and a Scanning Transmission Electron Microscope (STEM, ZEISS 018). High resolution Transmission Electron Microscopy (TEM) analysis was performed by a JEOL model JEM 3010-UHR, working at 300 kV (LaB_6 source) equipped with an OXFORD microanalysis GATAN photocamera.

Nitrogen adsorption-desorption at 77 K for specific surface area analysis was carried out on a Asap 2010 Micrometrics apparatus. Prior to adsorption, approximately 50.0 mg of solid were placed in the cell and evacuated at about 250 °C for 3 h.

X-ray photoelectron spectroscopy (XPS) measurements were performed with a PHI Versa Probe 5000 (Physical Electronics) spectrometer with a pass energy of 23.5 eV using the Al Kα as the exciting source of the X-ray. The internal correction of the binding energy was done using the adventitious C 1s peak near 284.6 eV.

The thermal stability of the samples was tested by thermo-gravimetric analysis (TGA), with a TGA/SDTA-851 instrument from Mettler, over a temperature range of 25-1000 °C under O_2 flux at a heating rate of 10 °C min^{-1}.

The glass transition temperature (*Tg*) of the materials was evaluated by differential scanning calorimetry (DSC) with a METTLER DSC-30 instrument, equipped with a low temperature probe.

Solid-state MAS-NMR spectra were acquired on a 400 MHz spectrometer (Bruker) using a 4 mm MAS probe (Bruker). ^{7}Li spectra were acquired with a single-pulse sequence, MAS frequency of 11 kHz, using a 90^{o} pulse of 5 μs, a recycle time of 0.5 s, and averaging over 2k acquisitions. The chemical shift reference is LiCl 1M. ^{27}Al spectra were acquired with a single-pulse sequence, MAS frequency of 11 kHz, using a hard pulse of 1 μs, a recycle time of 0.5 s, and averaging over 4k acquisitions. The chemical shift reference is Al^{3+} in aqueous solution. ^{13}C-^{1}H CP-MAS spectra were acquired at MAS frequency of 11 kHz, with a contact time of 3 ms, and a recycle time of 2 s. The chemical shift reference is TMS. The spectra were analysed with TopSpin package (Bruker).

The Fourier transform infrared spectroscopy (FT-IR, ThermoNICOLET Corporation, Nexus Model -670) was made at ambient temperature with a 8 cm^{-1} resolution.

The final thickness of the membranes was measured with a Mitutoyo Series 547 Thickness Gauge, equipped with an Absolute Digimatic Indicator (model IDC112XBS), with a resolution of ±1 μm and a max measuring force of 1.5 N.

The ionic conductivity at various temperatures (from 20 to 80 °C) of the NCPEs was measured using a PARSTAT-2273 potentiostat/galvanostat/frequency response analyser instrument (Princeton Applied Research, USA) in the 1 Hz to 100 KHz frequency range at the open circuit potential (OCV). Experiments were performed in hermetically sealed test cells (model ECC-Std, http://el-cell.com/products/testcells/ecc-std, from EL-Cell GmbH), fabricated inside an Ar-filled dry glove box (MBraun Labstar, Germany) having a humidity content below 1 ppm. The test cells were assembled by sandwiching a NCPE film between two SS-316 blocking electrodes (active area equal to 2.54 cm^2); a Teflon spacer was also used to avoid excessive deformation and major thickness variation upon temperature increase. Symmetric non-blocking cells of the type Li/NCPE/Li were also assembled for compatibility studies (interfacial stability), which was investigated by studying the time dependence of the impedance of the systems under open-circuit potential at 60 °C.

The lithium transference number was calculated by the method proposed by Vincent and co-workers.[1S] The following formula was adopted:[2S]

$$T_{Li}^{+} = \frac{I_{ss}(V - I_0 R_0)}{I_0(V - I_{ss} R_{ss})}$$

The Li/NCPE/Li cell was kept at 50 °C and polarized by a dc pulse of 20 mV. Time evolution of the resulting current flow was then followed. The initial (I_0) and steady state (I_{ss}) values of current flowing through the cell during the polarization were measured. R_0 and R_{ss} represent the resistance values before and after the perturbation of the system. Impedance spectra were made before and after the pulse application in order to correct the changes.

Clean electrodes and fresh samples were used for each of the above reported tests. To confirm the results obtained, the tests were performed at least three times on different fresh samples and cells.

Electrode preparation, lithium cell assembly and electrochemical characterization

The $LiFePO_4$/C cathode material was synthesized in the form of nanostructured powder through a mild hydrothermal procedure previously described in Meligrana et al.[3S] The composite cathode was prepared in the form of a film (average thickness of about 70 μm, calculated active material weight of about 2 mg) by blending 8 wt% of poly(vinylidene fluoride) as the binder (Solvay Solef 6020) with 10 wt% of acetylene black (Shawinigan Black AB50, Chevron Corp., USA) as the electronic conductivity enhancer and 82 wt% of $LiFePO_4$/C active material, thoroughly mixed in 1-methyl-2-pyrrolidone (NMP, Aldrich). The paste was coated by a doctor-blade process onto an aluminum foil current collector. After the complete evaporation of the NMP solvent by mild heating and progressive vacuum treatment for 24 h, electrode disks of 2.54 cm^2 were punched out and dried under high vacuum at 130 °C for 5 h.

The all-solid lithium polymer cells for the evaluation of the electrochemical characteristics were fabricated in the argon-filled dry glove box by laminating the three components in sequence, i.e., a lithium metal anode foil, a layer of the NCPE membrane and the $LiFePO_4$/C composite cathode film. The assembly was housed into a hermetically sealed test cell (ECC-Std). The characteristics and performance were investigated at 50, 60 and 70 °C in terms of charge/discharge galvanostatic cycling by an Arbin Instrument Testing System model BT-2000, setting the cut off potentials to 2.50–4.00 V *vs* Li^+/Li and the charge–discharge cycles at the same rates, ranging from C/10 to 5C (calculated on the basis of the theoretical specific capacity of 170 mAh g^{-1} for $LiFePO_4$). Charge reaction corresponds to lithium de-intercalation from the electrode material structure while discharge reaction corresponds to the lithium intercalation into the electrode material structure.

Clean electrodes and fresh samples were used for each of the above reported tests. To confirm the results obtained, the tests were performed at least three times on different fresh cells.

Characterisation of Al-BTC MOF

FT-IR analysis: evidences the formation of Al-BTC MOF (see FTIR analysis of the NCPEs in the followings for more detailed discussion).

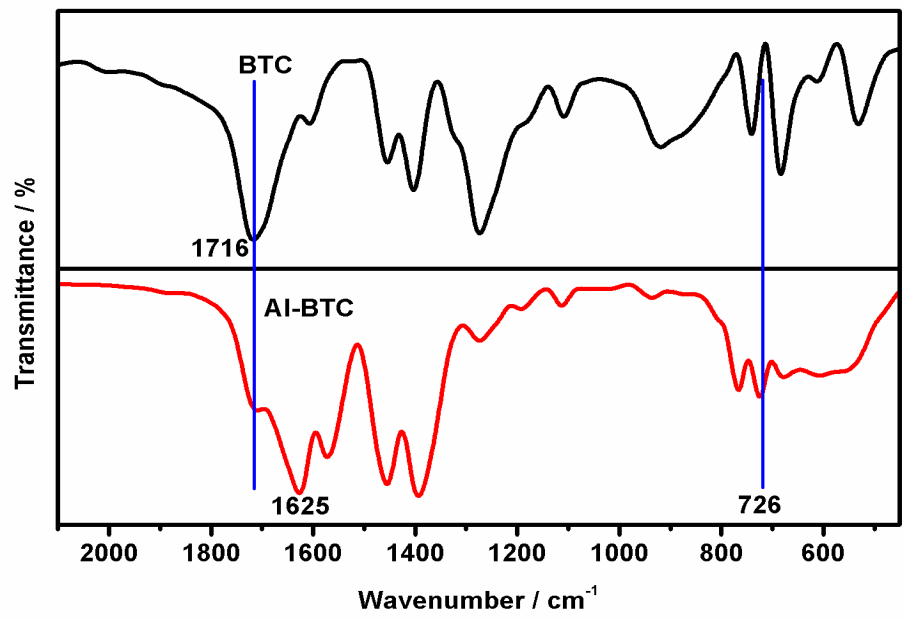

Figure S.2. Comparison between FT-IR spectra of BTC and Al-BTC MOF.

XRD analysis: presence of broad peaks mainly due to X-ray scattered from an amorphous phase and/or nano-crystals, in fact indicating that the crystalline component of the sample is rather low.[4S]

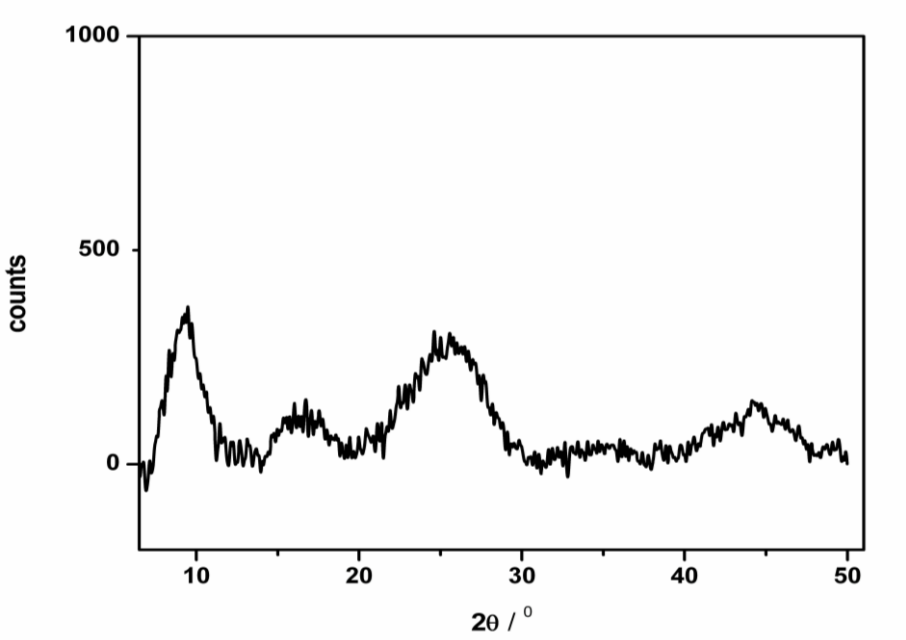

Figure S.3. Powder XRD analysis of Al-BTC(MOF).

FESEM / STEM analysis: a wormhole-like fluffy material, resembling a homogeneous aerogel-like body made of interconnected nanoparticles rather than fibres and/or crystal structures.[4S]

TEM / EDS analysis: nanostructured amorphous particles along with nano-crystals (see X-ray diffraction on a crystalline particle) well below 20 nm in diameter are observed, which are irregularly interconnected, spanning large void spaces.

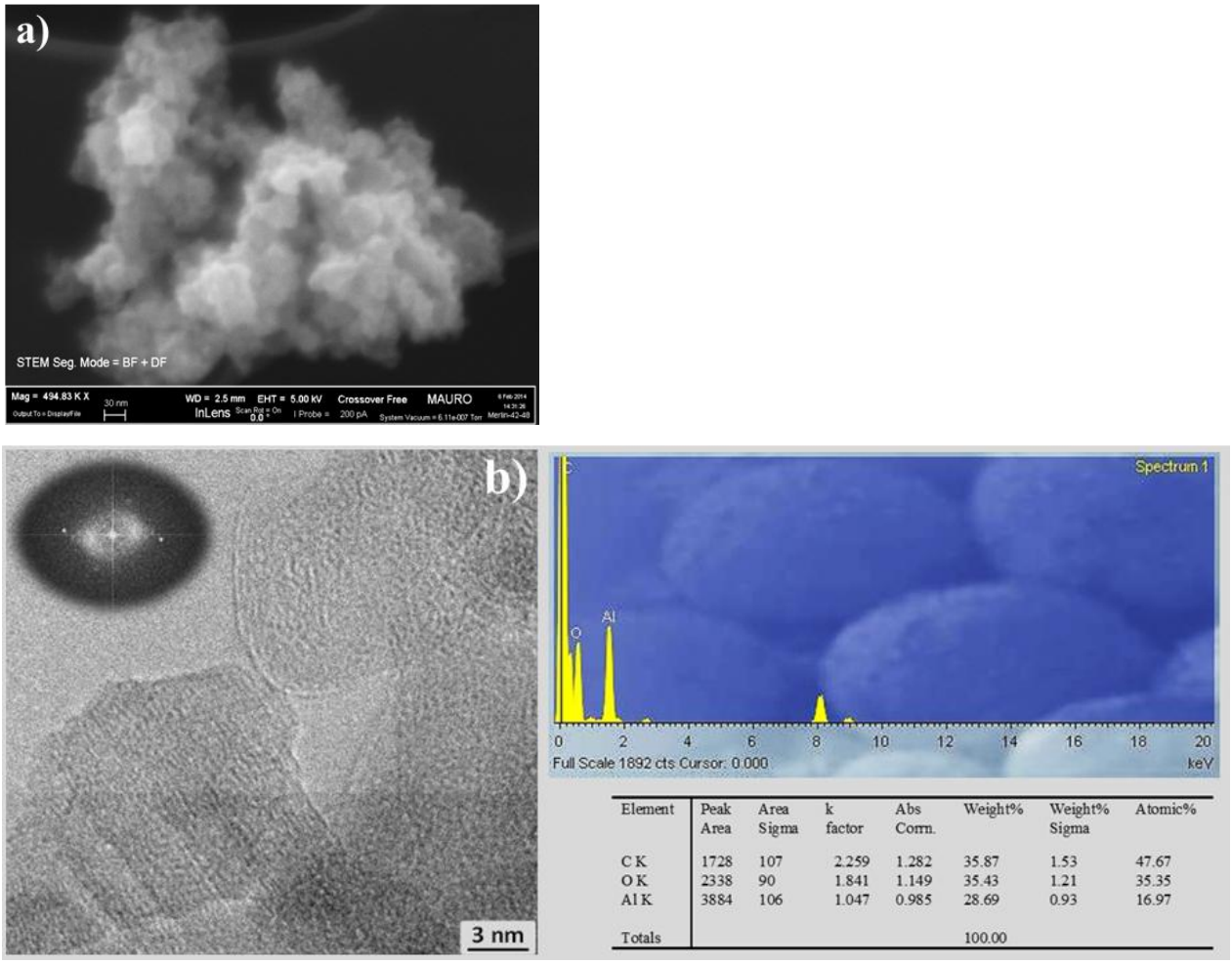

Element	Peak Area	Area Sigma	k factor	Abs Corrn.	Weight%	Weight% Sigma	Atomic%
C K	1728	107	2.259	1.282	35.87	1.53	47.67
O K	2338	90	1.841	1.149	35.43	1.21	35.35
Al K	3884	106	1.047	0.985	28.69	0.93	16.97
Totals					100.00		

Figure S.4. a) FESEM /STEM analysis of as-synthesized Al-BTC MOF after ultrasonic treatment, b) TEM analysis of as-synthesized Al-BTC MOF along with X-ray diffraction and EDS analysis on a selected particle.

N_2 physisorption at 77 K: mainly type II isotherm characteristics of non-porous materials with a clear hysteresis at high *P/P_0* values mainly ascribable to non-homogeneous inter-/intra-particle porosity and voids resulting from irregular connection between the nanoparticles during formation and aggregation. Some micro- (see the low *P/P_0* region) and meso-porosity (see the high *P/P_0* region) may be also present.[4S] Relatively high quantity of adsorbed gas accounting for the large surface area observed for a material having a non-homogeneous porosity.

Table S.2. List of the porous and surface properties of Al-BTC MOF.

Total Pore Volume	Average pore size (width)	BET Specific Surface Area	Langmuir Surface Area
0.52 $cm^3 g^{-1}$	53.56 nm	520 $m^2 g^{-1}$	695 $m^2 g^{-1}$

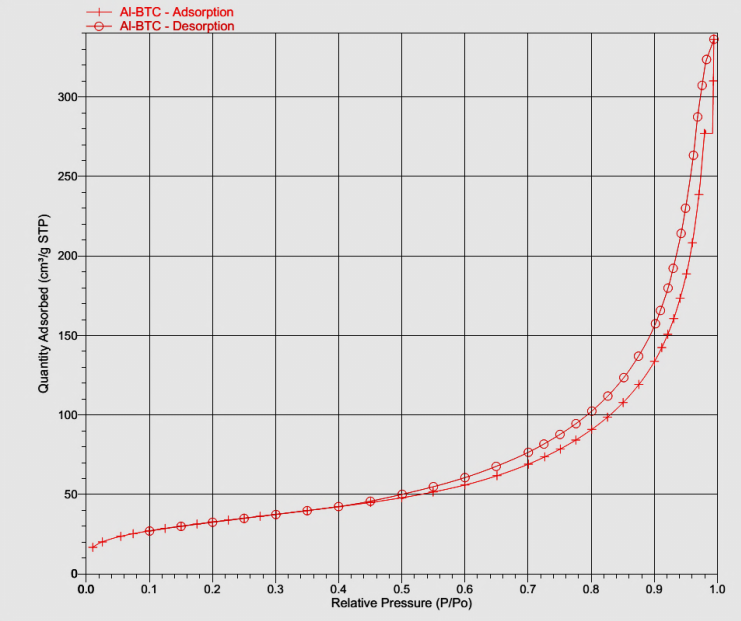

Figure S.5. Isothermal N_2 absorption-desorption curves for Al-BTC MOF.

TGA analysis: major weight losses observed in two steps. The slight shoulder at below 70 °C can be assigned to the removal of trapped solvent. The first major weight loss is ascribed to the continuous removal of water (free molecules trapped within the cavities and/or water bonded). It corresponds to almost 12 wt. % at 120 °C and almost 20 wt. % up to 300 °C, where the removal of chemisorbed H_2O molecules can be considered complete. The second weight loss is due to the decomposition of the structure with the release of the BTC species from ~ 400 up to ~ 650 °C. [5S] The final residue is constituted of nanoscopic (well below 20 nm as shown in the TEM image of Fig. S.8) highly defective nonstoichiometric aluminium oxides (confirmed by TEM/EDS analysis on the powder and the black colour of the residue) with a remaining weight of around 16 % of the initial value.

During TGA analysis, various aliquots of powder where collected at different temperatures as shown in Fig. S.6. Each sample was then subjected to TEM / EDS analysis. The experiment indicated that the morphological characteristics are preserved upon complete water removal; the chemical analyses gave atomic percentages for C, O and Al which were in good agreement with the chemical formula of the Al-BTC MOF up to 437 °C. Then, during the following main thermal

decomposition, the structure collapsed with release of BTC, as confirmed by the EDS analysis on both the 665 and 1000 °C samples (see the EDS analysis for the 1000 °C residue in Fig. S.7).

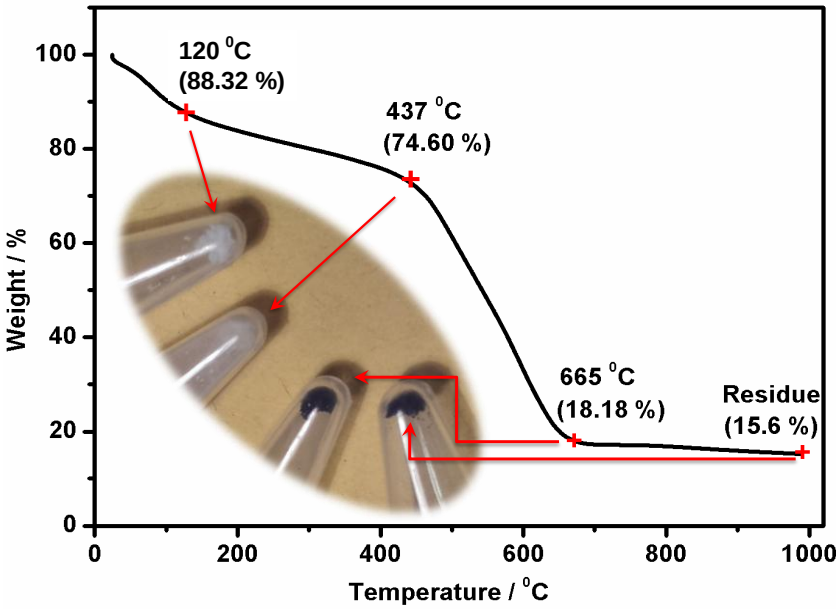

Figure S.6. Thermal stability of Al-BTC MOF along with depiction of the Al-BTC MOF powder during various thermal-decomposition stages.

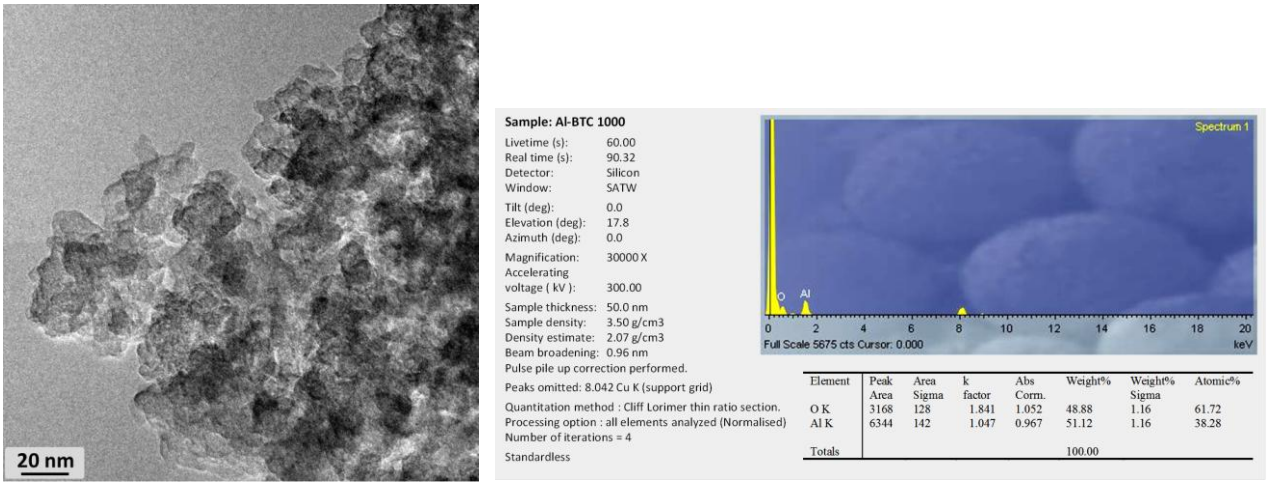

Figure S.7. TEM + EDS analysis of Al-BTC MOF after thermal decomposition at 1000 °C.

FESEM / STEM analysis of the NCPE (sample S4)

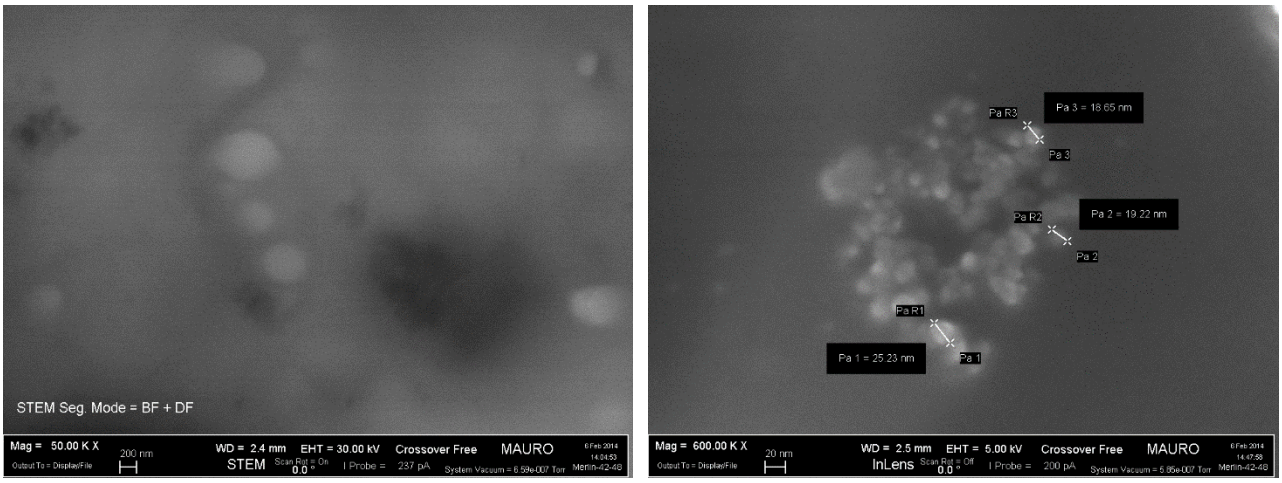

Figure S.8. FESEM /STEM analysis of the as-prepared Al-BTC(MOF, 10 wt. %) - laden MOF NCPE (sample S4) clearly evidencing that composites of PEO and MOF formed have nanosized domains.

Transference number of Li in PEO + Al-MOF (10 wt. %) + LiTFSI (NCPE)

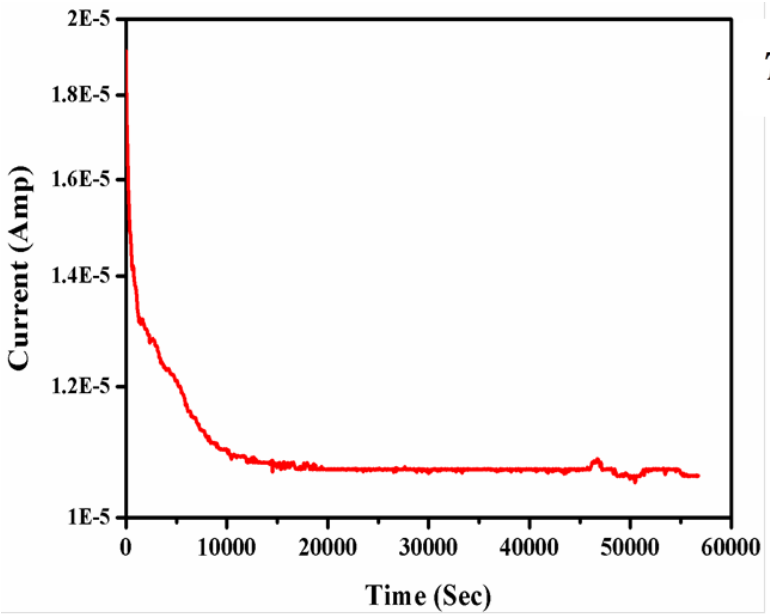

$$T_{Li}^{+} = \frac{I_{ss}(V - I_0 R_0)}{I_0(V - I_{ss} R_{ss})}$$

where

I - Current,

V - Applied potential,

R_b - Bulk resistance,

R_e - Interface resistance,

and 0 and ∞ refer to

the Initial and Steady-states,

respectively.

Figure S.9. Transference number of Li in PEO+MOF+LiTFSI – 0.55 (measured at 50 °C).[6S]

Interfacial resistance of Li/S4-NCPE/Li cell

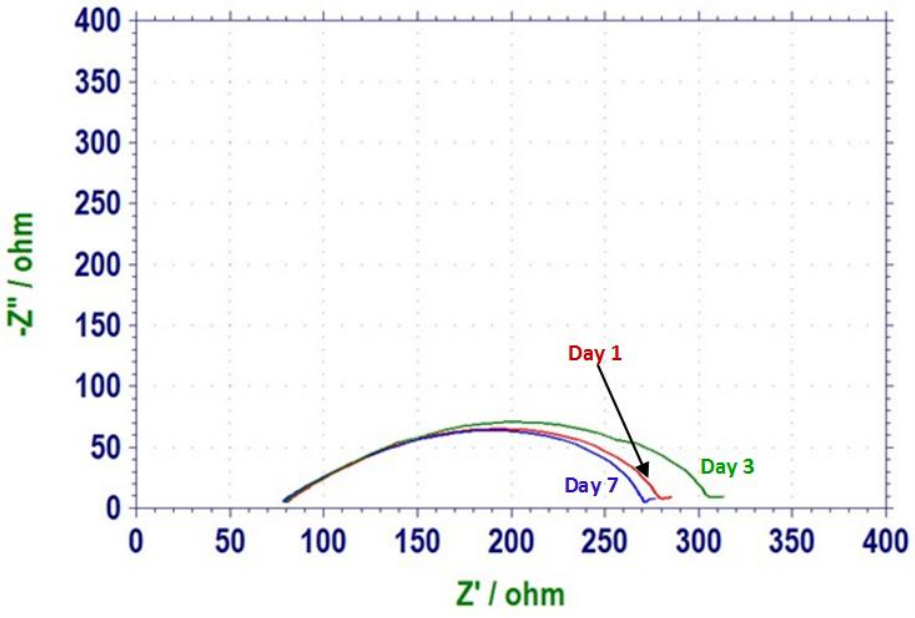

Figure S.10. Representative Cole-Cole plots for the Li/S4-NCPE/Li cell.

Al 2p XPS spectra of the as-prepared Al-MOF and MOF-laden NCPE

The binding energy value of Al-BTC MOF confirms the Al^{3+} oxidation state; slight shift towards lower binding energy values is observed in the Al 2p peak of the MOF-laden NCPE which may indicate an increase in the screening of the bound electron from the ion core.

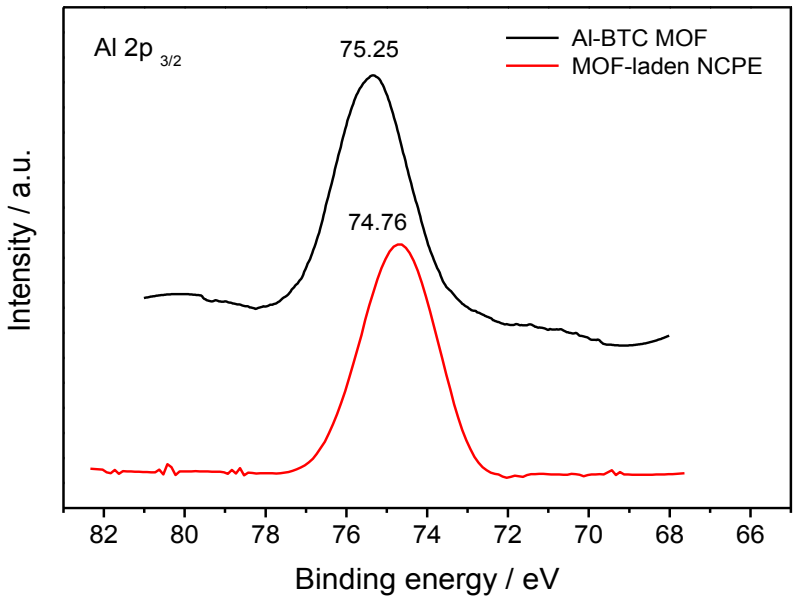

Figure S.11. X-Ray photoelectron spectroscopy analysis of Al-BTC MOF and NCPE.

Multinuclear solid-state NMR on Al-BTC MOF and nanocomposite membranes

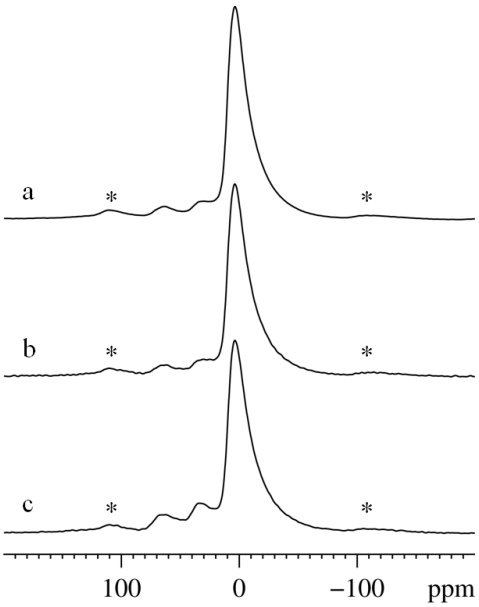

** spinning sidebands*

Figure S.12. Solid state NMR ^{27}Al MAS spectra a) Al-BTC(MOF), b) PEO+Al-BTC(MOF), c) PEO+LiTFSI+Al-BTC(MOF). No clear evidence of any interaction between the Al-MOF and the polymer and the salt.

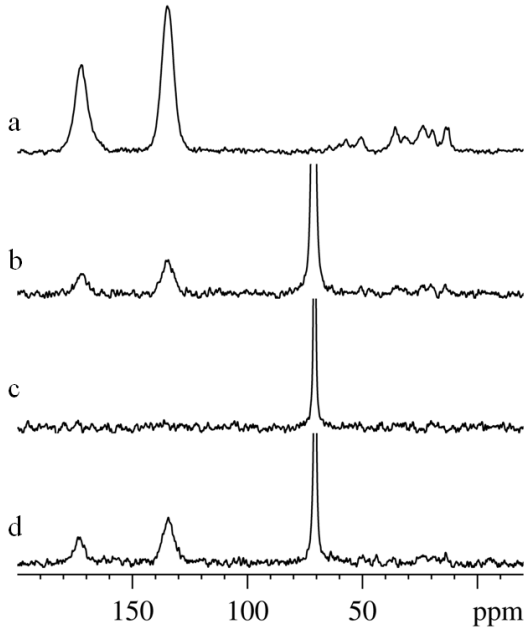

Figure S.13. Solid state NMR ^{13}C MAS spectra a) Al-BTC(MOF), b) PEO+Al-BTC(MOF), c) PEO+LiTFSI d) PEO+LiTFSI+Al-BTC(MOF). No clear evidence of any significant interaction due to the addition of Al-BTC(MOF) to the different samples.

FTIR analysis on Al-BTC(MOF) and nanocomposite membranes

The band that appears at 2886 cm^{-1} can be assigned to the –C–H stretching mode, and the peak at 1967 cm^{-1} is due to an asymmetric stretching mode. The peaks at 1466, 1103, 956 and 841 cm^{-1} are assigned to $–CH_2–$ scissoring, –C–O–C– stretching, $–CH_2$ twisting and $–CH_2–$ wagging modes, respectively. Also, PEO exhibits –C–H stretching (between 2800 and 2935 cm^{-1}), asymmetric stretching (1950–1970 cm^{-1}), asymmetric bending (1450 cm^{-1}), CH_2 scissoring (1465–1485 cm^{-1}), C–O–O stretching (1250–950 cm^{-1}), $–CH_2–$twisting (991 cm^{-1}) and $–CH_2–$ wagging (842 cm^{-1}).[7S-10S] In the spectra of pure PEO, the presence of the crystalline phase is indicated by the triplet peak of the C–O–C stretching vibration at ~1157, 1103, 1060 cm^{-1} with maximum at 1103 cm^{-1}.[10S-12S]

The FT-IR spectrum of Al-BTC(MOF) shows the vibrational bands in the usual range for the carboxylic function. Strong absorption bands, located at 1625 and 1571cm^{-1} and also between 1458 and 1385 cm^{-1} are assigned to bound C–O group, ν_{asym} and ν_{sym}, respectively, indicating that the BTC species is coordinated to aluminium. The strong and broad band centred at about 1716 cm^{-1} (please also refer to Figure S.2 where the BTC spectrum is shown) is characteristics of the –C=O stretching vibrations of the carboxylic –COOH group. The presence of broad O–H absorption peak between 3700–2500 cm^{-1} indicates that some of the carboxylic moieties are not fully deprotonated which, in turn, accounts for the presence of some free carboxylate not coordinated to Al centres. The peak at 1625 cm^{-1} confirmed that Al is coordinated with $–COO^-$ moieties. Nevertheless, such a peak is characteristics of coordination of Al with carboxylate group in the form of unidendate carboxylate which is attached to the metal. Moreover, a shoulder remains at 1716 cm^{-1}, less intense than in BTC spectrum, which confirms the non-complete coordination. The peak at 726 cm^{-1} indicates the –C=O deformation vibration which is shifted in the Al-BTC(MOF) profile as compared to the BTC one (see Figure S.2), accounting for the interaction of Al with the –C=O moiety. By comparison of the PEO+Al-BTC(MOF) and PEO+LiTFSI+Al-BTC(MOF) spectra, changes in the intensity, shape and position of the C–O–C stretching mode may be ascribed to the interactions between the polymeric chain and the filler; even if the peak overlapping in the nanocomposites might not be used as clear evidence of any interactions between the PEO ether group and the O–H acidic group.[5S]

When analysing the region between 800 and 600 cm^{-1} in the PEO+LiTFSI+Al-BTC(MOF) profile, less information may be clearly derived regarding the interaction between the three components of the NCPE. In fact, the bands generally used for the detection of $TFSI^-$ anions and/or ion pairing are located in this region but are overlapped with the peaks characteristics of Al-BTC(MOF) filler. Several bands located at 1280–1220 cm^{-1} are ascribable to different C–F stretching vibrations that, even if strong, are overlapped thus making any detailed analysis difficult.

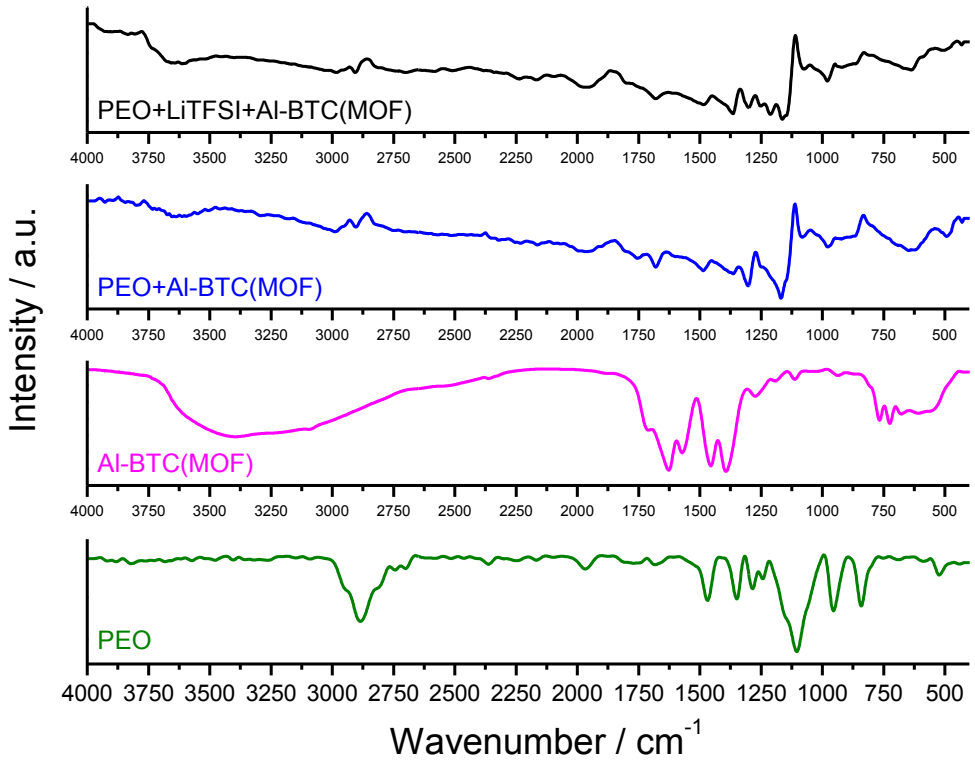

Figure S.14. Comparison of the FTIR analyses on PEO, Al-BTC(MOF), PEO+Al-BTC(MOF) and PEO+LiTFSI+Al-BTC(MOF), respectively.

Nevertheless, the presence of the salt is very evident when one considers the different intensity of the peaks situated in both the 1380–1310 and 680–480 cm^{-1} regions; these in fact are particularly sensitive to the $TFSI^-$ conformational state which is a constituent that is not present in PEO+Al-BTC(MOF).[13S,14S]

References

[1S] J. Evans, C.A. Vincent, P.G. Bruce, *Polymer*, 1987, **28**, 2324.

[2S] Y. Heo, Y. Kang, K. Han, C. Lee, *Electrochim. Acta*, 2004, **50**, 345.

[3S] G. Meligrana, C. Gerbaldi, A. Tuel, S. Bodoardo, N. Penazzi, *J. Power Sources*, 2006, **160**, 516.

[4S] L. Li, S. Xiang, S. Cao, J. Zhang, G. Ouyang, L. Chen, C.-Y. Su, *Nature Comm.* 2013, **4**, 1744(1-9).

[5S] T. Loiseau, L. Lecroq, C. Volkringer, J. Marrot, G. Férey, M. Haouas, F. Taulelle, S. Bourrelly, P.L. Llewellyn, M. Latroche, *J. Am. Chem. Soc.*, 2006, **128**, 10223.

[6S] F. Croce, L. Settimi, B. Scrosati, *Electrochem. Commun.*, 2006, **8**, 364.

[7S] S.E. Sloop, M. Lerner, *J. Electrochem. Soc.*, 1996, **143**, 1292.

[8S] S.M. Silverstein, C. Bassler, C. Morrill, *Spectrometric Identification of Organic Compounds*, John Wiley & Sons 1996.

[9S] A.M. Rocco, D.P. Moreira, R.P. Pereira, *Eur. Polym. J.*, 2003, **39**, 1925.

[10S] D.R. MacFarlane, P. Meakin, A. Bishop, D. McNaughton, J.M. Rosalie, M. Forsyth, Electrochim. Acta, 1995, **40**, 2333.

[11S] P. Chartoff, S. Lo Thomas, S.K. Harrell, R. Roc, *J. Macromol. Sci. Phys. B*, 1981, **20**, 287.

[12S] N. Angulakshmi, T. Prem Kumar, S. Thomas, A. Manuel Stephan, *Electrochim. Acta*, 2010, **55**, 1401.

[13S] M. Herstedt, M. Smirnov, P. Johansson, M. Chami, J. Grondin, L. Servant, J.C. Lassègues, *J. Raman Spectrosc.*, 2005, **36**, 762.

[14S] P. Johansson, *J. Phys. Chem. A*, 2001**, 105**, 9258.